RELAZIONE SCIENTIFICA STM 2016

Il Fruitore:

Dr. Mikhail Lisitskiy

Istituto di afferenza:

Istituto Superconduttori, Materiali Innovativi e Dispositivi (SPIN) del Consiglio Nazionale delle Ricerche, U.O.S di Napoli, Monte S. Angelo, Via Cinthia 80126 Napoli, Italy

con qualifica Ricercatore livello III

Descrizione dettagliata dell'Istituzione ospitante:

Physikalisches Institut, Karlsruhe Institute of Technology (KIT), Wolfgang-Gaede-Str. 1, D-76131 Karlsruhe, Germany. Fields of research: superconductivity, Josephson junctions and arrays, macroscopic quantum coherence, superconducting qubits, solitons in Josephson transmission lines, microwave spectroscopy, millimeter- and submillimeter wave experiments, low temperature laser microscopy.

Dipartimento di afferenza (tendina)

Physical Sciences and Technologies of Matter (Scienze Fisiche e Tecnologie della Materia).

Titolo del programma:

Strain tuning of individual two-level systems in AlN tunnel barrier detected by microwave spectroscopy of the NbN/AlN/NbN superconducting Josephson phase qubit.

Objects and purpose of the report

Referring to the planned activities provided by the STM 2016, the present document contains the description of the work done by Dr. Mikhail Lisitskiy together with Dr. Juergen Lisenfeld in the period of 15/05/2016-05/06/2016 in the Laboratory of Dr. Juergen Lisenfeld of the Physikalisches Institut, Karlsruhe Institute of Technology (KIT), Germany.

Introduction

Parasitic quantum two-level systems (TLSs) originating from structural dielectric material defects affect the functionality of superconducting quantum bits, because they decrease their coherence time [1]. Qubit spectroscopy was applied for the observation of coherent TLS for the first time in refs. [2,3]. The group of Prof. Ustinov at the KIT has developed a new technique for high-resolution defect spectroscopy by combining qubit spectroscopy with mechanical strain-tuning [4]. By this technique, the authors of [5] have demonstrated that minute deformation of the AlO_x tunnel barrier changes the energies of TLS and these changes have been registered by microwave spectroscopy of the superconducting qubit through coherent interaction between

these two quantum systems. Recently, the qubit spectroscopy incorporated with mechanical strain has been used for detection and full characterization of a system of two coherently interacting TLSs in an amorphous AlO_x material. By now all results have been obtained on Al based Josephson qubit and only relate to amorphous aluminum oxide barriers. Recently, NbN based Josephson qubits with an AlN tunnel barrier were fabricated by Dr. Lisitskiy in the SPIN-CNR, Italy, and tested in the KIT in terms of preliminary Rabi oscillation measurements. The STM 2016 grant of Dr. Lisitskiy was dedicated to carry out an experimental investigation in collaboration with the KIT of the NbN/AlN Josephson phase qubit, by qubit spectroscopy under mechanical stress with the objective to gain a better knowledge about the origin of decoherence in the AlN tunnel barrier.

Sample description, its installation and experimental setup

The superconducting Josephson phase qubit device was fabricated in a NbN-based technology developed by Dr. Mikhail Lisitskiy at the SPIN-CNR. Figure 1 shows an optical microscope photograph of the sample. The layout of the device was optimized in terms of improving the magnetic flux coupling between the flux bias coil and the loop of the qubit's rf-SQUID and minimizing the unwanted coupling to the dc-readout SQUID. In addition, the volume of the wiring insulation layers was as small as possible in order to decrease the number of possible TLSs which can contribute to the suppression of the qubit coherence time. The size of the qubit loop was chosen to result in a suitable β_L – parameter, which is determined by the critical current of the qubit Josephson tunnel junction and the loop inductance. The microwave transmission line for resonant qubit excitation was designed in coplanar configuration as a 6 μm wide central conductor separated from the ground planes by 4 μm. The central conductor was interrupted by a coplanar dc-break capacitor. As to

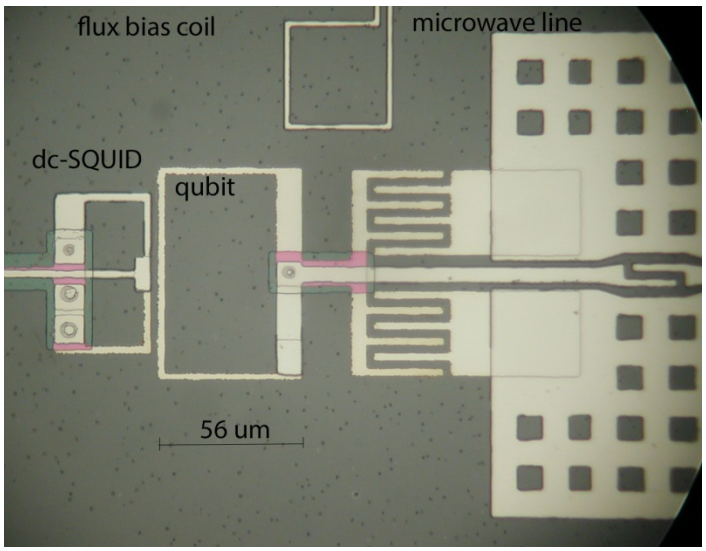

Figure 1. Optical microscope photograph of the NbN/AlN/NbN Josephson junction phase qubit circuit fabricated at SPIN-CNR and employed in the experiment in the KIT during the realization of STM 2016 program.

the ground configuration, the qubit was galvanically isolated from the microwave line by means of an interdigitated capacitor. This layout modification was meant to reduce the impact of quasiparticles which may be generated in the superconducting microwave line by stray infrared radiation being channeled to the sample from room temperature through the coaxial cable's Teflon insulation. The readout dc-SQUID was designed such that noise in its bias current does not couple to the qubit. For this aim, two identical Josephson junctions were connected in series in one branch of the SQUID, while a single junction was included in the other branch. The areas of each of the two junctions connected in series were twice as large as the area of the single junction. With this configuration, the SQUID's bias noise becomes decoupled from the qubit by tuning the dc-SQUID bias current until the inductances of both branches become equal, resulting in a vanishing mutual inductance between the dc-SQUID and the qubit. The NbN(200 nm) / AlN(3 nm) / NbN(60 nm) trilayer was deposited at room temperature on an R-plane sapphire substrate with a size of 10 mm x 10 mm in the MRC load-lock cryovacuum deposition system. The NbN bottom and top electrodes were made by dc-magnetron sputtering from an Nb target in Ar/N_2 atmosphere. The AlN barrier was deposited by dc-magnetron sputtering from an Al target in N_2 atmosphere. The first photoresist mask defining junction areas was patterned by conventional contact photolithography and the junction areas were defined by Reactive Ion Etching in an O_2+CF_4 plasma. The bottom NbN electrode was patterned by Reactive Ion Etching in O_2+CF_4 plasma after conventional contact photolithography. The wiring insulation SiO layer with a thickness of 30 nm was deposited by the thermal evaporation technique and its geometry was defined by a lift-off process. The NbN wiring layer of thickness 400 nm was deposited by dc-magnetron sputtering and patterned by a lift-off process.

A sketch of the main part of the experimental setup, namely a mechanical system to deform the sample for mechanical strain-tuning is reported in Figure 2(a). A voltage applied to the piezo actuator resulted in variable strain fields in the order of 10^{-7}/V [5]. Figure 2(b) shows a photograph of the real piezo actuator, where, similar to the sketch, it is possible to see clearly the metallic sphere between the piezo element and the sample substrate. The sphere serves to

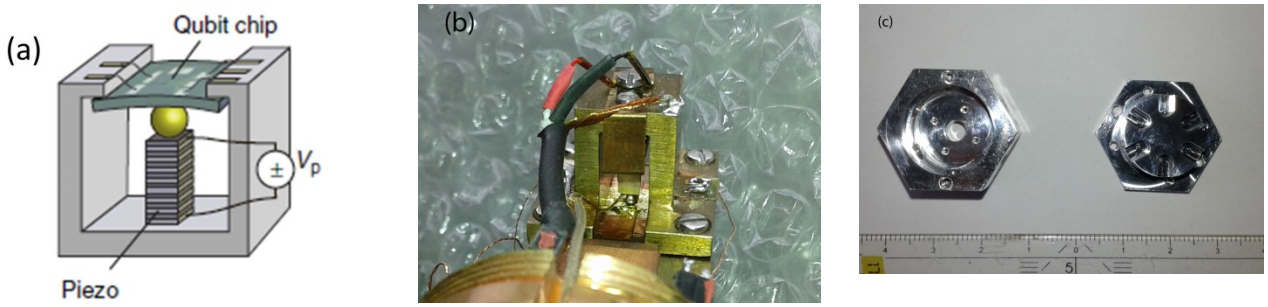

Figure 2.(a) Sketch of the piezo actuator (from [5]). (b) Photograph of the real piezo actuator. The object is rotated at 180°with respect to the sketch (a). (c) Photographs of the sample housing (left) and its cover (right). Both particulars are manufactured from Aluminum. The sample was installed inside the sample holder, which, in turn, was fixed on the piezo actuator. The central hole of the sample housing is designed for passing the piezo element and making a mechanical contact between the substrate and the metallic sphere.

avoid any lateral forces which might damage the piezo. The qubit chip was installed inside an Al sample housing shown in Figure 2(c). The sample housing was fixed on the piezo actuator and the piezo element with a metallic sphere were passed through a hole in the bottom of the sample housing. Simulations of the microwave response of the sample housing using a 3D finite-element simulation software (HFSS) show that the fundamental box resonance occurs around 12 GHz and first harmonics start above 18 GHz. Thin copper wires as well as coaxial cables entered the housing from the lateral holes and were soldered to cooper bonding pads. Aluminum bond wires were used to realize the connection to on-chip bonding pads. The magnetic shielding of the qubit was achieved by using superconducting Aluminum as a material for sample housing, which was additionally embedded in a closed cylinder made of cryoperm. The sample housing attached to the piezo actuator was thermally anchored to the mixing chamber of an Oxford Instruments Kelvinox He3/He4 dilution refrigerator which had a base temperature of about 40 mK. The cryostat was placed in a commercial shielded room, which was grounded but galvanically isolated from the gas handling system.

A schematic of the electronic circuit of the phase qubit of Figure 1 is shown in Figure 3(a). The qubit consists of a superconducting LC-resonator, realized by shorting a capacitively shunted Josephson element with an inductor. The resulting circuit is an rf-SQUID and is described by a double-well potential energy landscape – the dependence of the potential energy U on the phase difference across the Josephson junction φ (see Figure 3(b)). By adjusting the external magnetic flux bias applied on the integrated flux bias coil, one of the wells can be made shallow enough to contain only a small number of quantized energy levels. The first excited state $|1\rangle$ in this well can be populated by resonant absorption of photons from applied microwave pulses. After sending the microwave pulse (populating microwave pulse), a short but still adiabatic dc-flux pulse (readout dc pulse) is applied to the integrated flux bias coil, which raises the exited state close to top of the potential barrier and reduces the height of the barrier separating the wells. The pulse amplitude is adjusted such that a transition from the shallow to the deep well occurs only

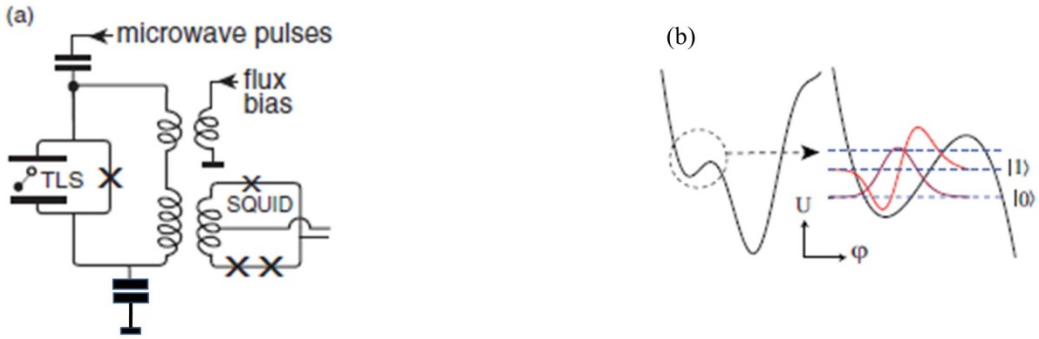

Figure 3. (a) Schematic electronic circuit of the phase qubit of Figure 1 (slightly revised from [6]). (b) Sketch of the qubit potential U(φ).On the right side, a zoom into the shallow left potential well indicates the wave functions describing the two qubit states $|0\rangle$ and $|1\rangle$ (from [7]). The configuration of the qubit potential is changed by the magnetic flux bias.

from exited states. The probability P_{esc} that the readout dc pulse leads to escape from the shallow well, which is experimental observable, hence directly reflects the population of the higher energy state. Since the wells differ by the circulation direction of the loop current, the

inter-well transition results in a change of magnetic flux, which is registered by recording the switching current of an inductively coupled readout dc SQUID. The operation of the single Josephson junction interferometer as a phase qubit is shown in Figure 4, indicating the sequence of flux bias signals Φ_q, microwave–pulse and bias current I_{DC_SQ} sent to the readout SQUID.

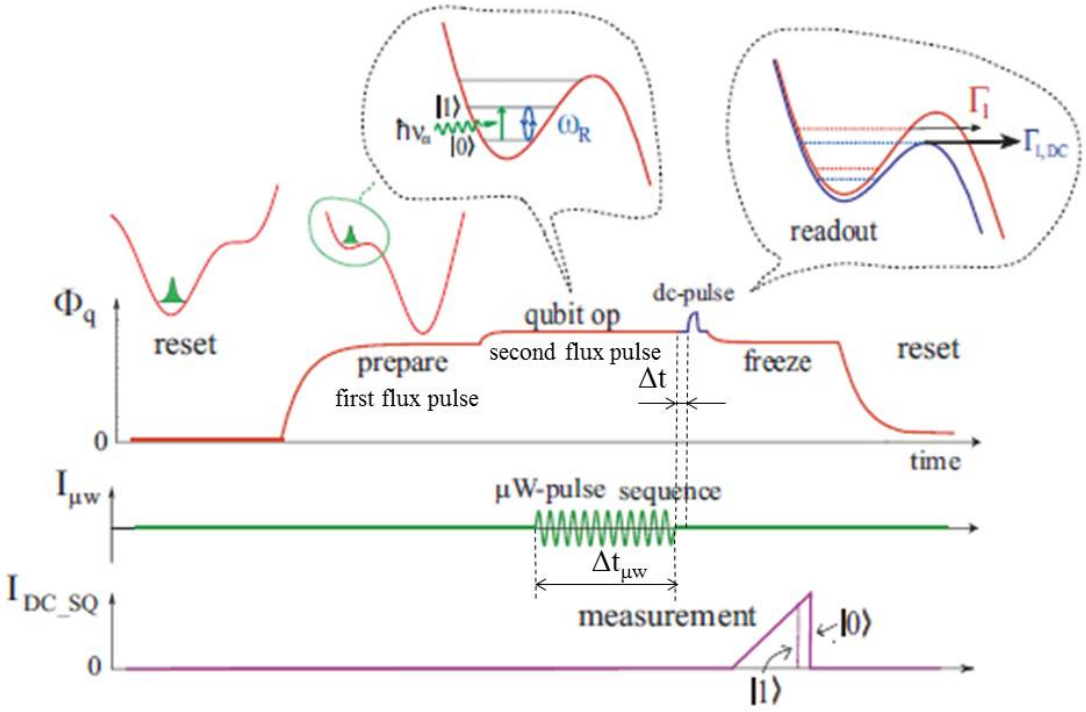

Figure 4. Time profiles of flux bias signals Φ_q, microwave pulse sequence $I_{\mu w}$ and bias current sent to the readout SQUID $I_{DC\ SQ}$ (from [8]).

Microwave qubit spectroscopy is used to find the energy difference between the ground and exited qubit states and consists of the measurements of the escape probability P_{esc} on microwave frequency at different values of the flux bias. It is important to note that during these measurements the amplitude of the second flux pulse is varied while the amplitude of the first flux pulse is kept constant (see Figure 4). In this way, the resonance frequency associated with the excitation of the qubit from the ground state $|0\rangle$ to the exited state $|1\rangle$ can be measured as a function of the flux bias. The usual representation of microwave spectroscopy data is a three dimensional plot, namely, flux bias (x-axis) vs. microwave frequency (y-axis) vs, P_{esc} (z-axis, color-coded).

Application of resonant microwaves induces Rabi oscillation between the two qubit states as long as the system remains coherent. The observation of these oscillations is a main test for macroscopic quantum coherence. To observe Rabi oscillations at a chosen microwave frequency, the value of the external flux bias corresponding to the qubit resonance peak is first

determined by microwave spectroscopy. The duration of the resonant microwave pulse $\Delta t_{\mu w}$ is then varied (see Figure 4), hereby adjusting the delay of the calibrated readout pulse such that it always occurs at the end of the microwave pulse. The probability to measure the qubit in the exited state P_{esc} is then plotted as a function of $\Delta t_{\mu w.}$ From the Rabi oscillation curve, the required duration for a so-called π-pulse is obtained as half the Rabi period. To directly measure the energy relaxation time T_1, the resonant microwave π-pulse is applied which is separated from the readout dc pulse by a variable delay time Δt. The value of T_1 is extracted from a fit resulting exponentially decaying escape probability.

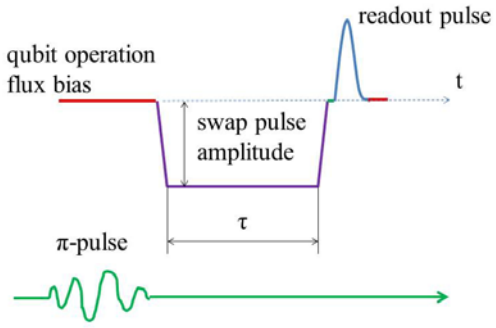

Figure 5. Pulse sequence used to detect individualTLSs via resonant interaction with a qubit.

Individual TLSs located in the dielectric of the thin tunnel barrier of the Josephson junction forming the qubit (Figure 3(a)), can be strongly coupled to the qubit via their electric dipole moment. This coupling manifests itself as an avoided level crossing in the qubit spectrum at flux bias values for which a certain TLS energy splitting ΔE matches the energy difference between the two qubit state [2]. The initial identification of TLSs and their coupling parameters are carried out by a so-called swap spectroscopy scheme based on the pulse protocol reported in Figure 5. Here, the qubit is first biased at a frequency far away from the intended spectroscopy region and exited by a resonant microwave π-pulse. Subsequent application of a flux pulse then modifies the effective flux bias, tuning the qubit to the probing frequency f_n where it resides for the holding time (see Figure 5). If at this frequency the qubit is at resonance with a certain TLS, the excitation is shared between both systems. This results in coherent oscillations that effectively swap the quantum states of the two systems at a frequency determined by their coupling strength. The procedure of the swap spectroscopy for TLS interaction consists in identification of qubit frequency far from an avoided level structure of the qubit spectrum, systematic measurements of the dependence of P_{esc} on time duration of the flux pulse τ for a range of probing frequencies f_n , i.e. for different values of the swap pulse amplitude. The effect of a coherent interaction between the TLS and the qubit is manifested by oscillations on the $P_{esc}(\tau)$ dependence. For a number of $P_{esc}(\tau)$ curves, the difference between $P_{esc}(f_n=0)$-$P_{esc}(f_n)$ is calculated for each values of τ. This value decreases if the qubit is in resonance with a TLS,

which thus presents an observable by which the frequencies of TLS in the sample can be detected. It is important to note that the $P_{esc}(\tau)$ dependence at $f_n=0$ (i.e. far away from any resonant TLS) corresponds to the energy relaxation for the isolated qubit, which is used for the measurement of the energy relaxation time T_1. This procedure is repeated for a range of piezo voltage to vary the mechanical strain applied to the sample.

The low-frequency signals of the qubit flux bias and dc-readout SQUID bias were provided by custom-made analog electronics. In order to minimize heating that occurs during the readout dc-SQUID's operation, its bias current was set back to zero immediately after each switching event. A digital pulse was used in order to start and stop the ramp of the bias current. The whole pulse sequence comprising qubit operation and SQUID readout was repeated at rate of 300 times per seconds. The microwave pulses and their sequence were formed by modulating a continuous microwave signal (generated by an Agilent E8257C microwave source) using a mixer, to which the desired pulse envelope is fed from an Arbitrary Waveform Generator (Tektronix AWG5014B). The same generator was used for application of dc-readout pulses and flux pulses for qubit spectroscopy experiments. For Rabi oscillation measurements with high time resolution, the generator Agilent 81130A was used instead of the generator Tektronix AWG5014B.
The measurement computer controlled microwave and pulse generators and received the data from the time counter via a GPIB interface. An extensive software package has been developed in Matlab to program arbitrary parameter sweeps and allow for fast on-line data evaluation. It also featured one-click data fitting, automatic readout pulse calibration routines and a large variety of plotting possibilities.

Experimental results and discussion

The experiment was started with a check of the sample quality by the measurements of the current-voltage curve of the dc-readout SQUID (Figure 6).

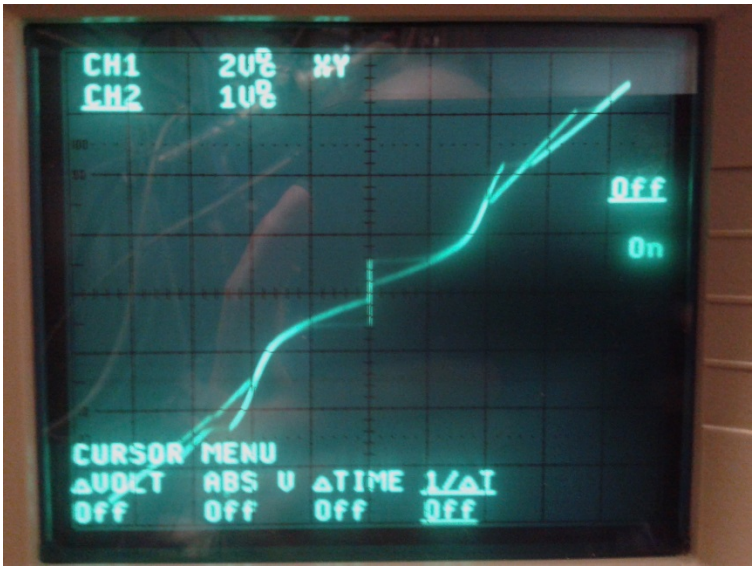

Figure 6. Current-voltage curve of the dc readout SQUID as observed on an oscilloscope. Voltage is a horizontal axis: 2 mV/div. Current is a vertical axis: 0.02 mA/div. T=60 mK.

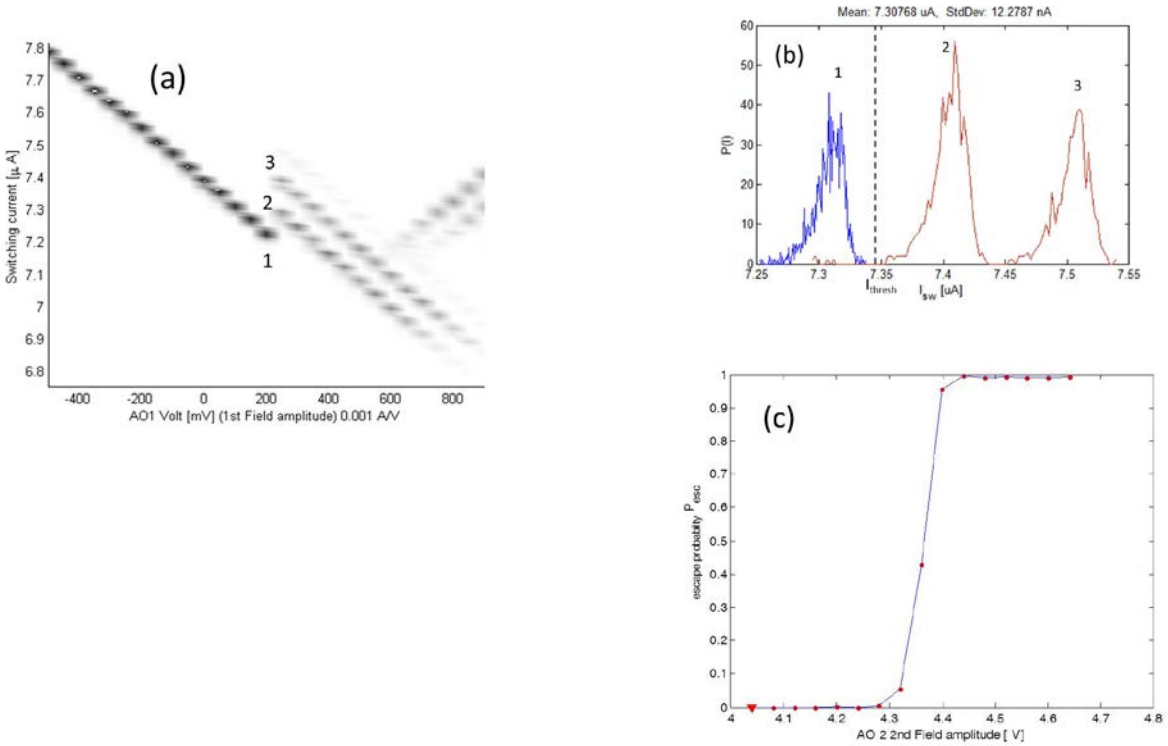

Figure 7. (a) Current positions of histogram peaks of the switching current distribution as a function of the first external magnetic flux pulse for the asymmetric dc-SQUID coupled to the qubit (left plot). External magnetic flux is in arbitrary units. (b) Switching current distributions measured at a magnetic flux near 200 a.u. The peaks number 1, 2 and 3 correspond to the critical current number 1,2 and 3 in Figure (a), respectively. Peak 1 is associated with the left potential well, the presence of peaks 2 and 3 originates in multiple right wells. I_{thresh} is a threshold value of the switching current used for calculation of the escape probability P_{esc} from left well to any right one (2 or 3). (c) Dependence of P_{esc} on second flux pulse at fixed value of the amplitude of the first flux pulse. Here, P_{esc} changes from 0 to 1, which confirms that the dc-SQUID can discriminate between qubit flux states with 100% contrast.

Before qubit spectroscopy measurements, a suitable flux bias pulse level for qubit operation (operation flux pulse amplitude) is first set (see Figure 4). For this, the dependence of the dc-SQUID switching current on external magnetic flux was measured in order to obtain the discrete steps resulting from qubit undergoing transitions between potential wells at certain values of the external flux (in the most simplest case, this occurs between left and right wells, as shown in Figure 3(b)). Two flux pulses were used for these measurements, which were generated by two current sources connected in parallel and set to different output ranges in order to increase the available resolution. Figure 7 (a) shows one of the results of switching current measurements by varying the coarse (first) magnetic flux pulse amplitude. The step around 200 a.u. indicates the qubit switching between wells, and thus a suitable flux value for qubit operation is just before the step. The switching current distributions recorded at magnetic fluxes near 200 a.u. are plotted in Figure 7(b). In general, for correct qubit readout it is important to have an initial single peak in the switching current distribution (corresponding to complete qubit initialization in a single left well). A threshold value of the switching current was determined, as shown in Figure 7(b) and the escape probability P_{esc} (or $P(|1\rangle)$) that the qubit is a flux state corresponding to the right potential well, was calculated as the number of counts above this threshold divided by the

total number of events. The dependence of P_{esc} on magnetic flux was precisely measured by varying the amplitude of the second flux pulse and by using the first flux pulse with a certain constant amplitude as an offset (see Figure 7(c)).
Most attention in the experiment was devoted to optimize the experimental conditions for qubit spectroscopy measurements. Figure 8 shows the result of the microwave power scan of P_{esc} as a function of microwave frequency. The multitude of peaks which appear at high power levels is due to parasitic resonances in the microwave circuitry.

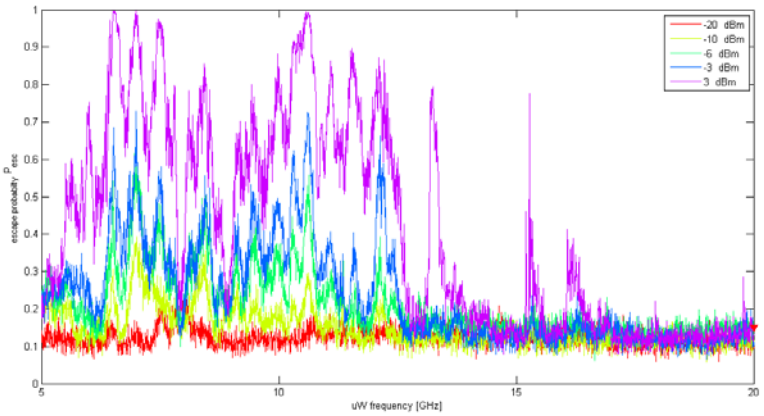

Figure 8. P_{esc} vs. microwave frequency, measured at different values of the microwave power.

Great effort was made in order to minimize the presence of parasitic resonances on qubit spectra. One spectrum measured after this optimization procedure is shown in Figure 9(a). In this plot, the magnetic flux bias is indicated on the x-axis as the voltage that was applied to the voltage–controlled current source, whereas 1 V corresponds to approximately 20 µA. At each flux level, the microwave frequency was swept only around the expected resonance position (blue range) in order to decrease the total measurement duration. Figure 9(b) reports P_{esc} vs.

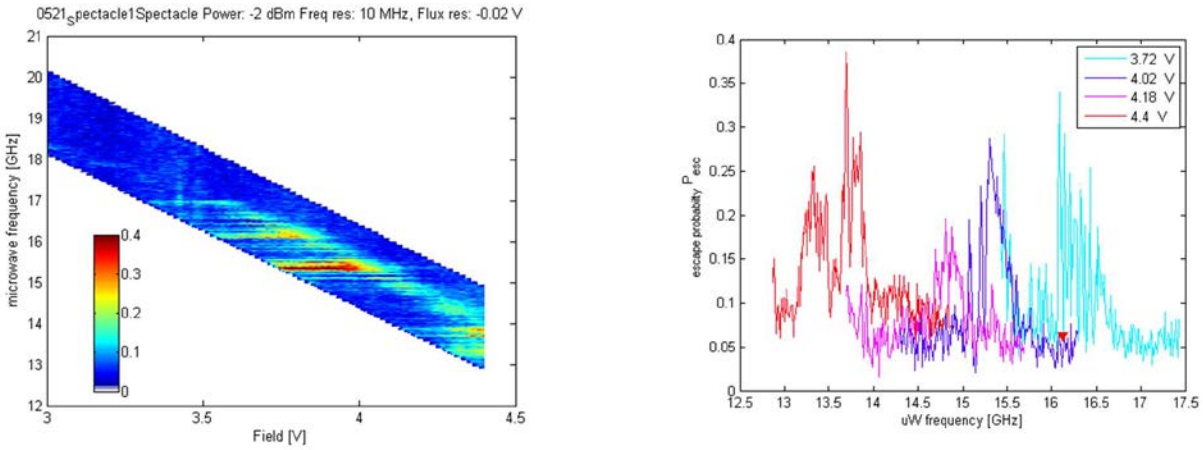

Figure 9. (a) Qubit microwave spectroscopy result after careful adjustment of the measurement procedure. Magnetic field (i. e. flux bias) is in arbitrary units. (b) P_{esc} vs, microwave frequency traces recorded at different values of the flux bias (from spectra (a)). Qubit resonances are visible together with parasitic resonances.

microwave frequency curves at several values of the flux bias related to spectra of Figure 9(a). The qubit resonant peaks are shifted by variation of the flux bias. Namely by this way it was possible to distinguish qubit resonances from unwanted parasitic ones. Figure 10(a) shows another qubit spectroscopy data obtained in the full frequency range, whereas the other conditions were identical to the measurements shown in Figure 9(a). The parasitic resonances are clearly seen at about 15.3 GHz and 16.1 GHz. The spectrum of Figure 10(a) clearly shows qubit resonances located along the black line. Especially good resonances are observed at frequencies below 15 GHz. Gaps at certain frequencies are presumably due to the strong resonant coupling of the qubit to individual TLS but can also arise from the frequency dependence of the microwave transmission line.

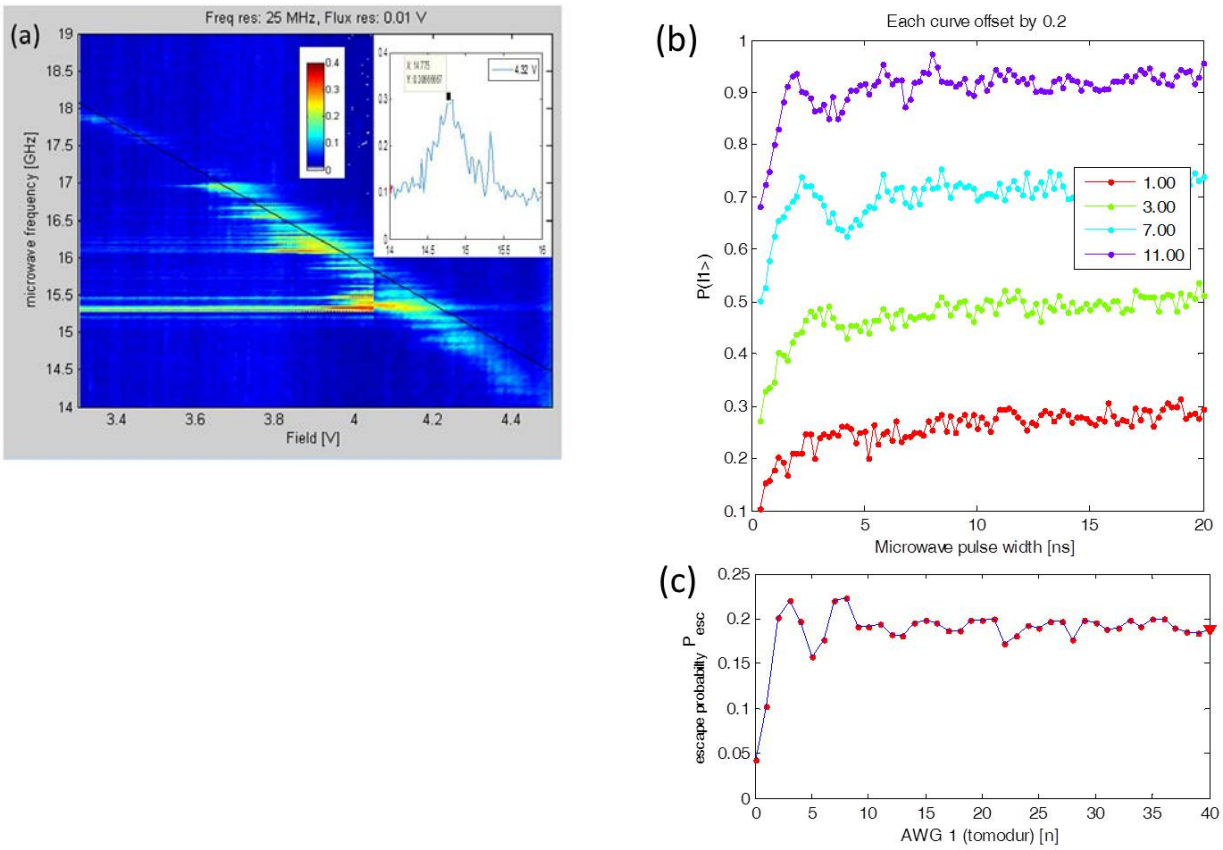

Figure 10.(a) Qubit spectrum measured for wide range of the microwave frequency at optimized conditions identical to the measurements of the spectrum of Figure 9(a). The x-axis is flux bias in arbitrary units. The insert reports P_{esc} vs. microwave frequency at a flux bias of 4.32 V (a.u), which was used in following measurements of Rabi oscillation. (b) Rabi oscillations measured at a resonance frequency of 14.775 GHz and at different microwave powers. The power values are indicated in the legend. The generator Agilent 81130A was employed for these measurements due to its higher time resolution of 2 ps. (c) Repetition of the Rabi oscillation measurement by Arbitrary Waveform Generator Tektronix AWG5014B (1 ns time resolution) at a microwave power of 7 dBm.

The qubit resonance frequency of 14.775 GHz at a flux bias of 4.32 V (a.u) was chosen from the spectroscopy data of Figure 10(a) as a promising working point in order to measure Rabi oscillations. For observation of Rabi oscillations, the generator Agilent 81130A was used because of its higher time resolution, and P_{esc} was measured as a function of microwave pulse

widthand at different microwave powers (Figure 10 (b)). As can be seen from Figure 10 (b), clear Rabi oscillations were recorded at power exceeding 3 dBm. The nicest Rabi oscillation curve was obtained for a power of 7 dBm. From this curve the π-pulse duration of 2-3 ns was estimated as a half of the Rabi oscillation period. Afterwards, the generator Agilent 81130A was exchanged by Arbitrary Waveform Generator Tektronix AWG5014B and the measurement of the Rabi oscillations was repeated (see Figure 10(c)) to confirm that no excess noise originates in the Tektronix device.

To directly measure the energy relaxation time T_1, the microwave π-pulses with $\Delta t_{\mu w}$=3 ns at a resonance frequency of 14.775 GHz were applied and P_{esc} was measured at different values of the delay time Δt between the π-pulse and the dc readout pulse (Figure 11(a)). The value of T_1 of 10.13 ns was extracted from the fit of the experimental dependences by the exponential function describing the decaying escape probability.

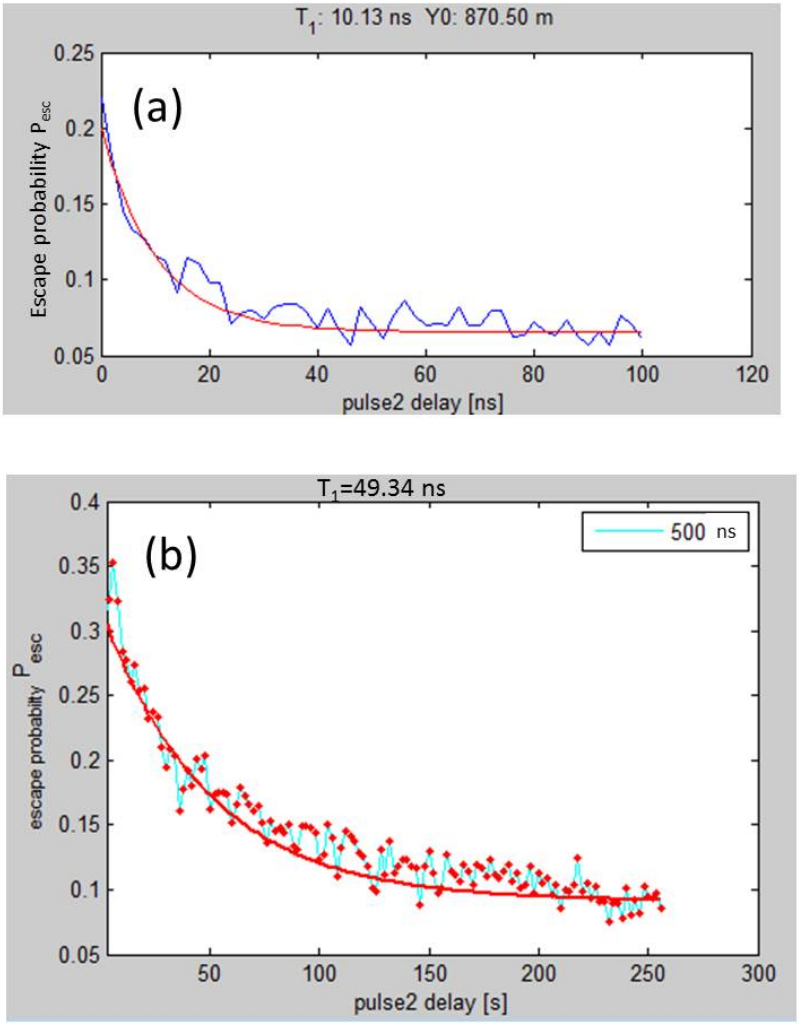

Figure 11. Escape probability P_{esc} vs the delay time between populating microwave pulse and readout dc pulse at different microwave pulse duration $\Delta t_{\mu w}$: (a) π-pulse ($\Delta t_{\mu w}$=3 ns), T_1=10.13 ns; (b) $\Delta t_{\mu w}$ = 500 ns, T_1=49.34 ns.

It was found that the increase in the microwave pulse duration results in the increase of the energy relaxation time T_1. For example, for microwave pulse duration $\Delta t_{\mu w}$ = 500 ns the estimated T_1 is of 49.34 ns (Figure 11 (b)). This effect may in principle originate in the fact that for longer microwave pulses, more TLS become saturated (excited) by the microwave directly, which thus cannot anymore absorb energy from the qubit.

In order to measure the dependence of T_1 on qubit frequency, we applied flux pulses after the qubit was excited (Figure 5) to detune the qubit. Here, we used a microwave pulse duration of 500 ns. Figure 12 (a) shows the P_{esc} vs. τ dependence recorded at a constant flux pulse amplitude of -0.33 V. The dependence of the energy relaxation time T_1 on the flux pulse amplitude is shown in Figure 12(b). In such a measurement, low values of T_1 (dips) indicate resonant coupling to TLS at the corresponding frequencies. Coherent coupling to individual TLS results in oscillations on the otherwise purely exponential qubit decay (green curve in Figure. 12 (a)), which also spoils the exponential fit and thus results in large error bars as seen in Figure. 12 (b) at certain frequencies.

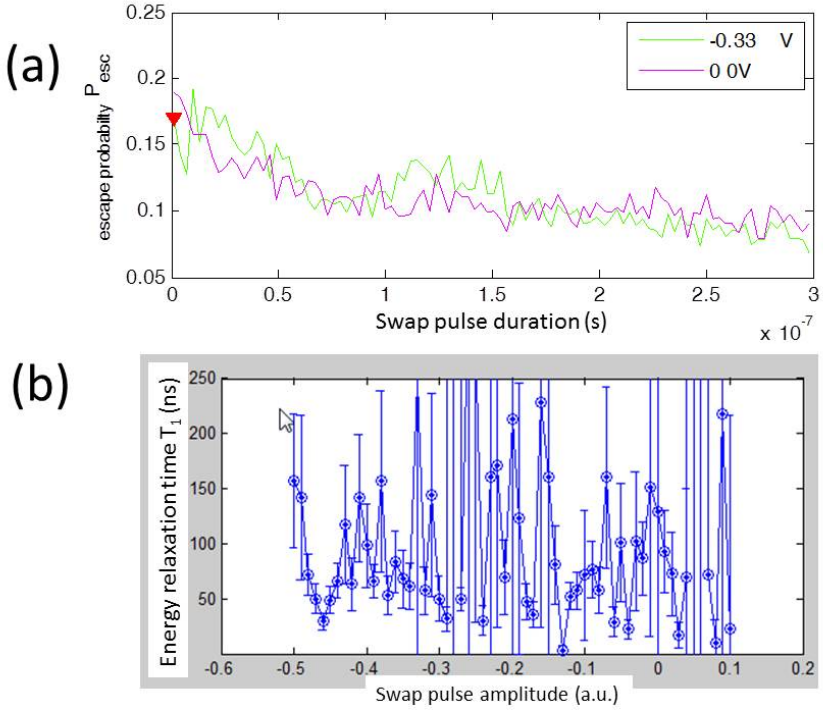

Figure 12. (a) P_{esc} vs flux pulse duration for different flux pulse amplitudes indicated in the legend; (b) Dependence of the T_1 on the flux pulse amplitude.

When we first applied a voltage to the piezo actuator, magnetic flux was trapped in the readout SQUID or its electrodes. The control measurement of the dependence of the switching current distribution on the first external magnetic flux pulse showed the curve which was different from that plotted in Figure 7 (a). Since motion of the trapped fluxon resulted in excess noise, we had to warm up the sample to remove the trapped fux.

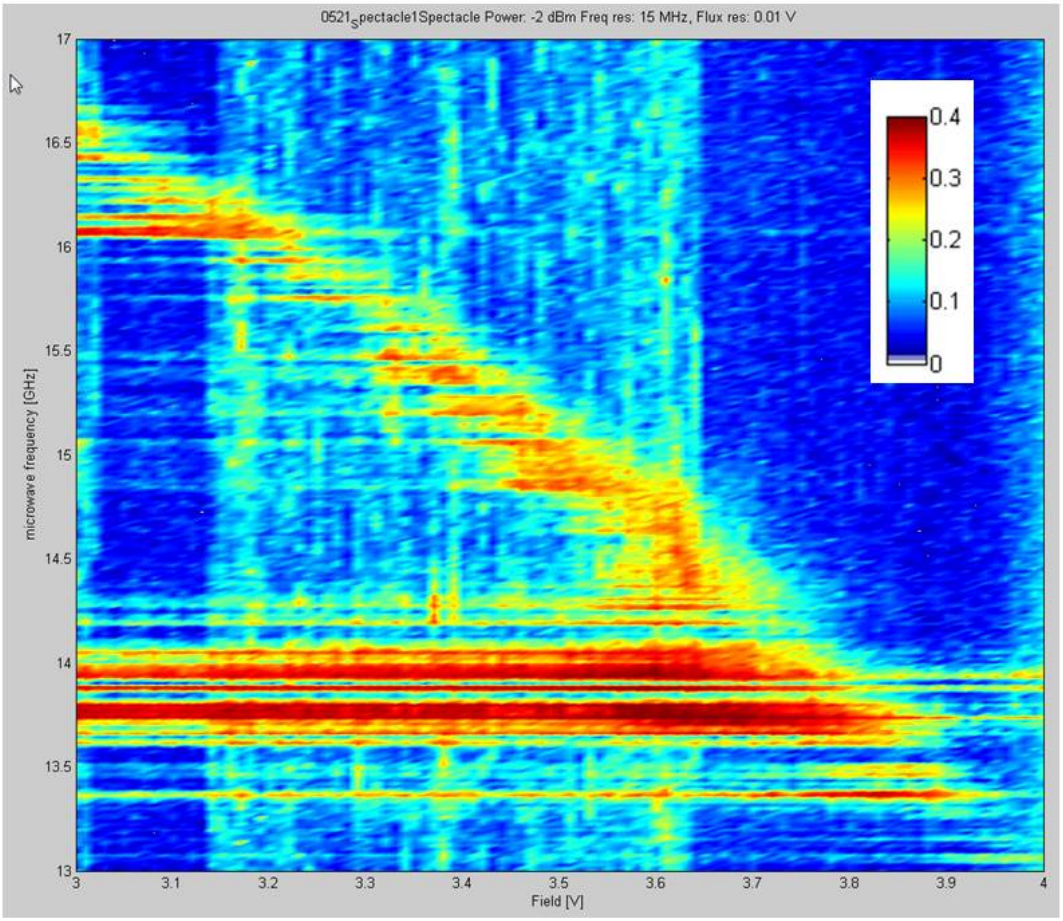

Figure 13. Qubit spectrum measured after heating of the sample up to $T>T_c$ and subsequent cooling up to 40 mK. Similar to spectra of Figure 9(a) and Figure 10(a), the x-axis is the flux bias in arbitrary unit.

Thus, the qubit was warmed up to T~20 K ($T>T_c$ of NbN) and cooled down to 40 mK in zero external magnetic field. Thereupon measurement parameters were adjusted for the new initial magnetic trapping conditions and the qubit spectroscopy was again repeated. Figure 13 shows the best result of the qubit spectroscopy obtained after one heating-cooling cycle of the cryostat. The spectrum after the thermal cycling is characterized by a large amount of parasitic resonances in contrast to the previous spectrum reported in Figure 10(a). A main part of parasitic resonances of the spectrum of Figure 13 are localized at frequencies from intervals between 13.4 GHz and 14.3 GHz and between 16.0 GHz and 16.6 GHz. So, the frequency positions of parasitic resonances are different from the spectroscopy carried out at the beginning of the experiment (compare Figure 13 and Figure 10(a)). Taking into account the difference in the frequency positions of parasitic resonances and the different magnetic patterns of switching current before and after heating-cooling process, it is possible to consider the magnetic flux trapped in superconducting films of the NbN qubit as a possible source of parasitic resonances. Such a behavior after heating-cooling processes was not observed on Nb and Al based qubit samples measured before in the same experimental setup. This difference can be described by the higher capability of NbN material to trap Abrikosov vortices as a strong

second type superconductor in comparison with Al (conventional first type superconductor) and Nb (soft second type superconductor).

Substantial attention was devoted to a detailed investigation of the energy relaxation time T_1 on different physical parameters and conditions such as the microwave pulse duration, the microwave power and the way to apply the microwave pulse. Figure 14 (a) shows a measurement of P_{esc} as a function of the delay time between populating microwave pulse for different microwave pulse duration $\Delta t_{\mu w.}$ (Figure 14 (a)).

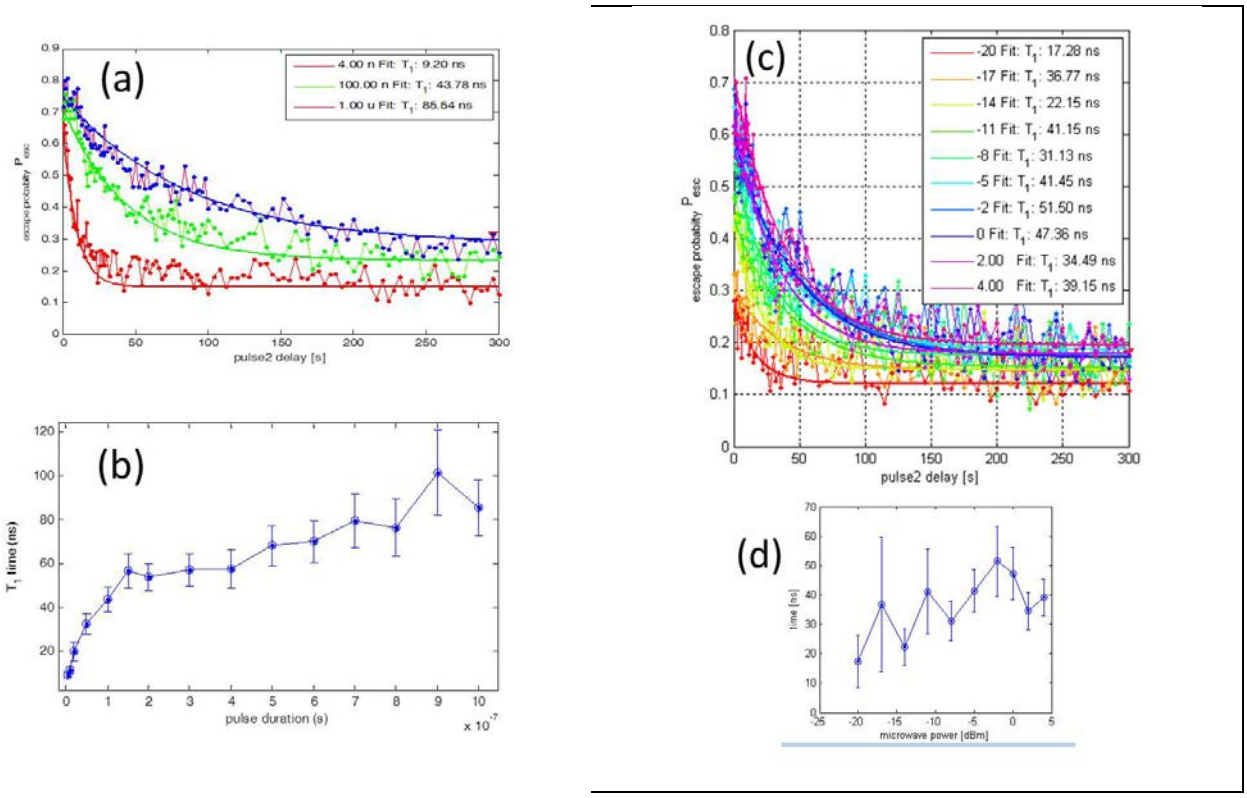

Figure 14. Test of the dependence of the energy relaxation time T_1 on the microwave pulse duration (a-b) and on microwave power (c-d) at the constant microwave frequency of 14.89 GHz. (a) Results of systematic measurements of the P_{esc} vs the delay time between the microwave pulse and the dc readout pulse carried out at different values of the microwave pulse duration. (4 ns, 100 ns and 1 μs). Solid lines are the results of fitting procedure for finding of the T_1; (b) Dependence of the T_1 on the microwave pulse duration extracted from the set of measurements plotted in Figure (a). (c) Measurements of the P_{esc} vs the delay time between the microwave pulse and the dc readout pulse at constant value of the microwave pulse duration of 300 ns and at different microwave power from -20 dBm to 4 dBm; (c) Experimental dependence of the T_1 on the microwave pulse duration extracted for the dependences of Figure (c).

For clarity of data presentation, only three curves measured at microwave pulse duration of 4 ns, 100 ns and 1 μs are reported in Figure 14(a). T_1 was extracted from these data by fitting to exponentials, which is plotted as a function of the microwave pulse duration in Figure 14(b). Figure 14(b) shows that T_1 increases with the microwave pulse duration and that at the pulse duration of 1.5×10^{-7} s the trend of the curve is changed from a rapid increase to a slow one. The microwave pulse duration of 300 ns was chosen for investigation how the energy relaxation

time depends on the microwave power (here, the microwave frequency was of 14.89 GHz) (Figure 14(c)). It was found that the decay time T_1 increase with microwave power from 17 ns up to 40 ns (see Figure 14(d)). The populating microwave pulse was substituted by the sequence of π-pulses (4 ns duration each) separated from each other by a delay time of 24 ns. The decay time T_1 was measure after final π-pulse. Figure 15 (a) shows the pulse protocol used for this measurement. The number of π-pulses was varied and for each value of the number of π-pulse the T_1 was measured. It was found that the energy relaxation time T_1 increases with number of π-pulses and this behavior was similar to the increase with the microwave pulse duration (Figure 15 (b)).

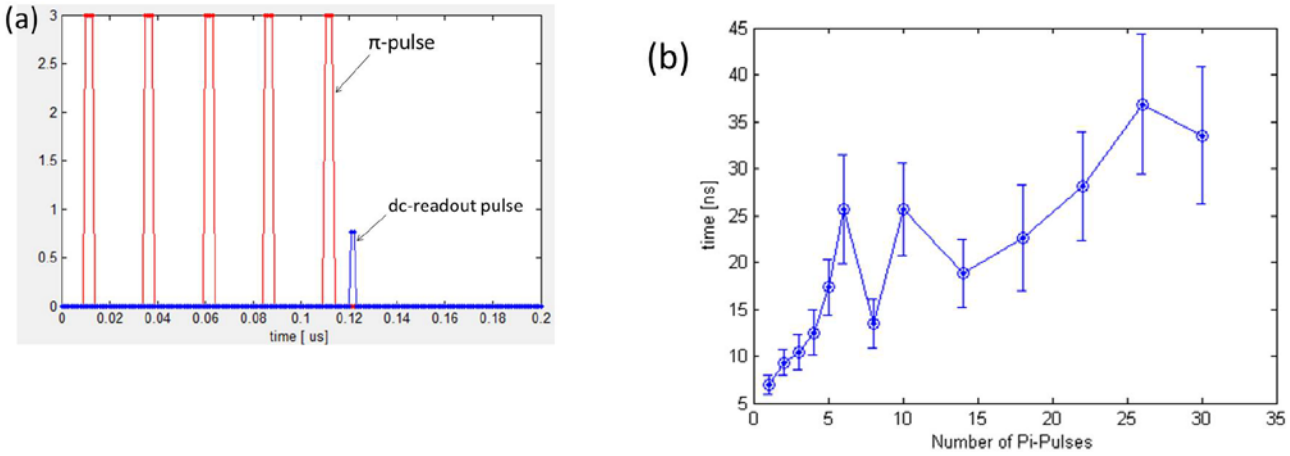

Figure 15. (a) Pulse protocol for substitution of a populating microwave pulse by a sequence of π-pulses separated from each other by a determined delay time. (b) Dependence of the T_1 on the number of of π-pulses measured by the pulse protocol reported in Figure 16 (a). Here, the delay time between π-pulses was 24 ns, the π-pulse duration was 4 ns, the microwave pulse frequency was 14.9 GHz, and the microwave power was 0 dBm.

To investigate the influence of the mechanical strain on the energy relaxation time T_1, we measured T_1 at different piezo voltages ranging from 0 to 4.8 V in increments of 0.1 V. Figure 16(a) reports the dependence of P_{esc} on Δt recorded at piezo voltages of 1.4 V, 2.4 V and 3.4 V. Only insignificant variations of T_1 were observed when the piezo voltage was varied. The complete dependence of the T_1 on the piezo voltage is shown in Figure 16(b). Taking into account the experimental error reported in Figure 16(b), it is difficult to conclude about the effect of the mechanical strain on the energy relaxation time T_1.

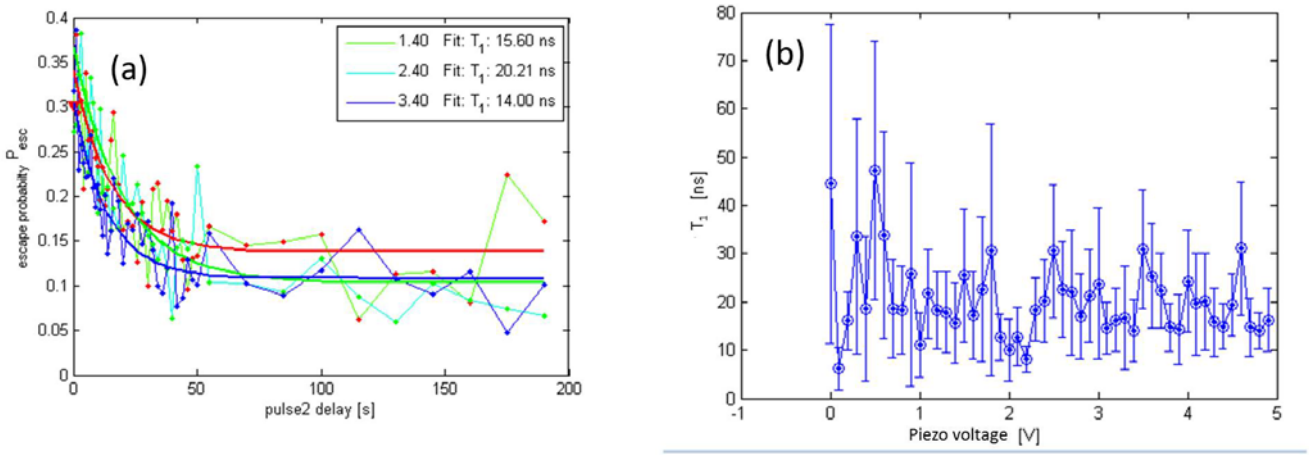

Figure 16. (a). The escape probability P_{esc} as a function of the delay time between populating microwave pulse and dc readout pulse at piezo voltages of 1.4 V, 2.4 V and 3.4 V. (b) The complete dependence of T_1 on the piezo voltage.

To determine T_1 as a function of qubit frequency for zero applied piezo voltage, we performed a swap spectroscopy experiment. For this, the escape probability P_{esc} was recorded as a function of the swap pulse amplitude at different flux pulse duration τ (see Figure 5). The results obtained for four values of τ are shown in Figure 17. The experimental dependencies shown in Figure 17 manifest as a rapid P_{esc} decay for large swap amplitudes greater than 0.3 V. As to observation of the effect of TLSs, unfortunately no evidence of the resonant interaction

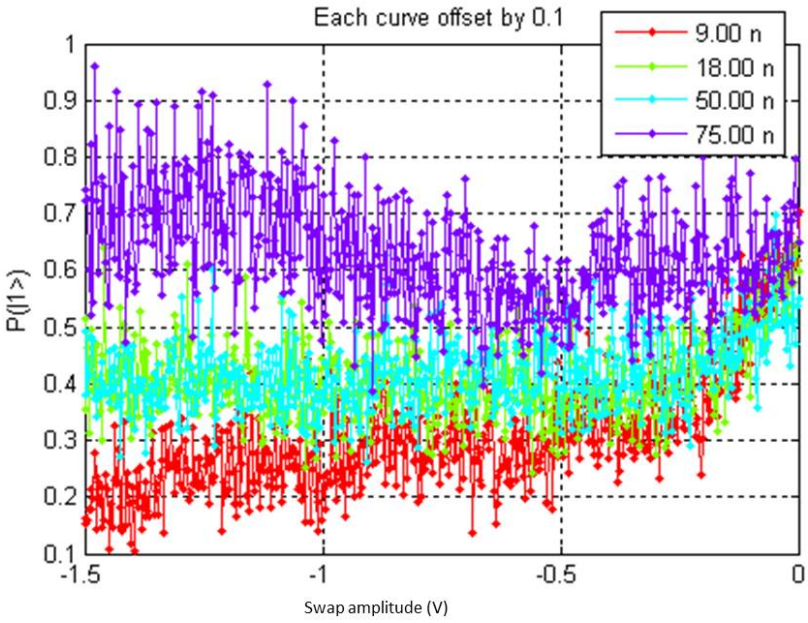

Figure 17. Dependence of the escape probability P_{esc} on the swap pulse amplitude for different swap pulse durations as indicated in the legend.

between TLS and the qubit was observed, which would manifest as pronounced dips at certain swap pulse amplitudes. The intrinsic qubit coherence time less than 10 ns seems to be short for observation of the coherent interaction between the qubit and single TLSs. In addition, a possible high density of TLSs inside the AlN barrier is presumably another reason for the absence of clearly distinguishable TLS resonances.

Conclusions

The coherent resonant properties of the NbN/AlN/NbN Josephson phase qubit were studied with a focus on the interaction between the qubit and individual TLSs localized in the AlN tunnel barrier. Most attention was devoted to optimize the experimental conditions for qubit spectroscopy measurements, in particular, to minimize the presence of parasitic resonances on qubit spectra. The qubit spectra recorded after the adjusting procedure manifested avoided level crossings which seem to be attributed to the qubit coherent interaction with TLSs. The size of the splitting in terms of frequency was very small. Thermal cycling of the sample beyond its superconducting transition temperature T_c and subsequent cooling to T=40 mK gave rise to a change in qubit spectra, consisting in the appearance of different parasitic resonances and a shift of the offset magnetic flux. In addition, thermal cycles resulted in changes in the shape of the magnetic pattern of the switching current of the readout dc-SQUID. From these observations, one can conclude that magnetic flux trapped in NbN superconducting films of the qubit device presents a possible source of the parasitic resonances. In general, the NbN qubit demonstrated a higher susceptibility of trapping magnetic flux as compared to Nb and Al based qubit devices. Clear Rabi oscillations were observed in the present sample. The observation of Rabi oscillations confirmed the macroscopic quantum behavior of the NbN/AlN/NbN qubit. The oscillations decayed after a mean time of about 3-4 ns. We performed systematic studies of the qubit coherence time T_1 on different physical conditions such as microwave power, different number of applied π-pulse, and different values of mechanical strain. The qubit relaxation time T_1 was found to depend on the duration and power of the applied microwave pulse as well as their number, reaching values up to 100 ns for long pulses or high microwave powers. This effect may in principle originate in the fact that for longer microwave pulses, more TLS become saturated (excited) by the microwave directly, which thus cannot anymore absorb energy from the qubit. No evident change in T_1 was observed for different mechanical strain. The physical reason of the increase of the qubit relaxation time T_1 with the microwave pulse duration is still unknown and its search requires further detailed investigation. Different attempts to carry out the swap spectroscopy of single TLSs were done at zero piezo voltage. Unfortunately, no evident pronounced dips on the resonant curves associated with coherent interaction between the qubit and single TLSs, could be observed. The intrinsic qubit coherence time of less than 10 ns seems to be too short in order to carry out the high-resolution TLS spectroscopy. Another explanation of the absence of individual TLS resonances can be an unexpectedly high density of TLSs inside the AlN barrier.

References

[1] Robert McDermott et al., "Materials Origins of Decoherence in Superconducting Qubits" IEEE Trans. Applied Superconductivity, Vol. 19, 2-13 (2009).

[2] R.W. Simmonds et al., "Decoherence in Josephson Phase Qubit from Junction Resonators" Phys. Rev. Lett., Vol. 93, 077001-1-07003-4 (2004)

[3] John M. Martinis et al., "Decoherence in Josephson Qubit from Dielectric Loss" Phys. Rev. Lett., Vol. 95, 210503-1-210503-4 (2005)

[4] Grigori J. Grabovskij et al., "Strain Tunning of Individual Atomic Tunneling Systems Detected by a Superconducting Qubit", Science, Vol.338, 232-234 (2012)

[5] Juergen Lisenfeld et al., "Observation of directly interacting coherent two-level systes in an amorphous material", Nature Communications, DOI: 10.1038/ncomms7182 (2015).

[6] J. Lisenfeld et al., Phys.Rev. Lett., Vol.105, 230504 (2010).

[7] J. Lisenfeld et al., Phys. Rev. Lett., Vol. 99, 170504 (2007).

[8] J. Lisenfeld, "Experiments on Superconducting Josephson Phase Quantum Bits", PhD Thesis, Physikalisches Institut III, Friedrich-Alexander-Universität Erlangen-Nürnberg, 2008.

Pozzuoli, 25 July 2016

Dr. Mikhail Lisitskiy